Journal Pre-proofs

Temperature Dependence of Cu(I) Oxidation and Cu(II) Reduction Kinetics in the Selective Catalytic Reduction of NO_x with NH_3 on Cu-Chabazite Zeolites

Siddarth H. Krishna, Casey B. Jones, Rajamani Gounder

PII: S0021-9517(21)00351-1
DOI: https://doi.org/10.1016/j.jcat.2021.08.042
Reference: YJCAT 14308

To appear in: *Journal of Catalysis*

Received Date: 1 July 2021
Revised Date: 9 August 2021
Accepted Date: 17 August 2021

Please cite this article as: S.H. Krishna, C.B. Jones, R. Gounder, Temperature Dependence of Cu(I) Oxidation and Cu(II) Reduction Kinetics in the Selective Catalytic Reduction of NO_x with NH_3 on Cu-Chabazite Zeolites, *Journal of Catalysis* (2021), doi: https://doi.org/10.1016/j.jcat.2021.08.042

Temperature Dependence of Cu(I) Oxidation and Cu(II) Reduction Kinetics in the Selective Catalytic Reduction of NO_x with NH_3 on Cu-Chabazite Zeolites

Siddarth H. Krishna, Casey B. Jones, Rajamani Gounder

Charles D. Davidson School of Chemical Engineering, Purdue University, 480 Stadium Mall Drive, West Lafayette, IN 47907, USA

*Corresponding author: rgounder@purdue.edu

Abstract

The selective catalytic reduction (SCR) of NO_x with NH_3 over Cu-exchanged chabazite (CHA) zeolites at low temperatures (<523 K) occurs via a redox mechanism in which O_2 oxidizes two NH_3-solvated Cu^I sites, and NO and NH_3 react together to reduce NH_3-solvated Cu^{II} sites. Increasing the Cu ion density in Cu-CHA zeolites increases the kinetic relevance of Cu^{II} reduction relative to Cu^I oxidation during SCR at fixed gas pressures, given the dual-site requirement of Cu^I oxidation but the single-site requirement of Cu^{II} reduction. Apparent activation energies (E_{app}) measured at fixed gas pressures increase with Cu ion density, at first glance suggesting that Cu^I oxidation has a lower E_{app} value than Cu^{II} reduction, assuming mean-field kinetic behavior wherein barriers are independent of Cu site density. Here, steady-state SCR rates were measured at varying O_2 pressures (1–60 kPa) and temperatures (446–501 K) to isolate E_{app} values for Cu^I oxidation and Cu^{II} reduction on Cu-CHA samples of varying Cu ion density (0.065–0.35 Cu per 10^3 Å^3), revealing instead that E_{app} values depend on Cu density for both Cu^I oxidation and Cu^{II} reduction steps. E_{app} values for Cu^I oxidation increase monotonically with Cu density in the full range studied, while E_{app} values for Cu^{II} reduction are invariant with Cu density except at the lowest Cu densities (0.065–0.10 Cu per 10^3 Å^3). Moreover, the small differences between E_{app} values for Cu^I oxidation and Cu^{II} reduction indicate that their kinetic relevance depends only weakly on temperature for a given Cu-CHA sample. These findings sharply contrast the conclusions from previously reported E_{app} data measured at fixed gas pressures and interpreted using mean-field kinetic descriptions, and illustrate the importance of measuring rate data over wide ranges of reaction conditions and sample compositions to more precisely describe the non-mean-field kinetic behavior of NH_3-solvated Cu ions that become mobilized in zeolites during low-temperature SCR catalysis.

Highlights

- Rates of NO_x SCR redox cycle depend on Cu ion density and kinetic regime
- Langmuirian kinetic model describes SCR rates at varying O_2 pressure and temperature
- E_{app} values for both Cu^I oxidation and Cu^{II} reduction depend on Cu density
- Kinetic relevance of Cu^I oxidation and Cu^{II} reduction depends weakly on temperature
- Changes in E_{app} with Cu ion site density reflect non-mean-field kinetic behavior

Keywords

apparent activation energy, Cu-zeolites, Cu(I) oxidation, Cu(II) reduction, dynamic multinuclear sites, heterogeneous catalysis, non-mean-field behavior, NO_x selective catalytic reduction

TOC Graphic

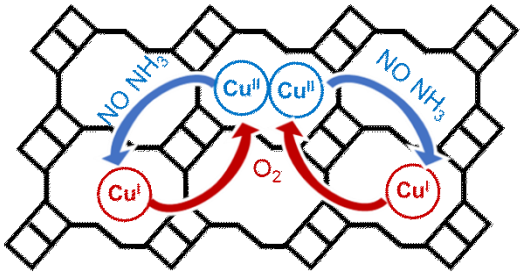

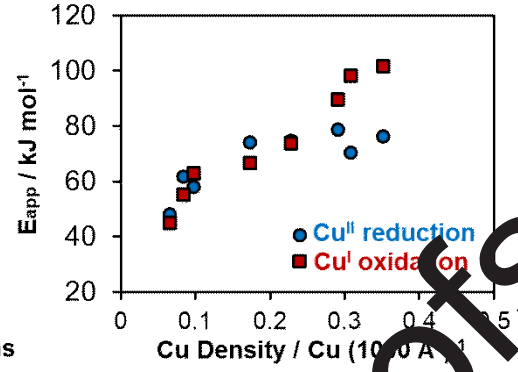

Apparent activation energies for NO_x SCR depend on Cu ion density under both Cu^I oxidation- and Cu^{II} reduction-limited conditions

1. Introduction

The selective catalytic reduction (SCR) of nitrogen oxides (NO_x, x = 1,2) with NH_3 using Cu-exchanged chabazite (CHA) zeolites is a commercial technology to mitigate NO_x emissions in diesel and lean-burn engines [1,2]. The majority of NO_x emissions occur at low engine exhaust temperatures (<523 K) corresponding to cold-start and low-load conditions [3,4]. In this low-temperature regime, NH_3 solvates and mobilizes Cu ion sites [5–10] to facilitate a redox mechanism in which two $Cu^I(NH_3)_2$ complexes react with O_2 to form binuclear O-bridged NH_3-solvated Cu^{II} complexes in the SCR oxidation half-cycle [11–14], while NO and NH_3 react together to reduce NH_3-solvated Cu^{II} complexes to $Cu^I(NH_3)_2$ in the SCR reduction half-cycle [5,15–17]. A deeper understanding of the reaction mechanism, kinetically relevant steps, and active site requirements under low-temperature reaction conditions would provide practical guidance on catalyst design and operation strategies to further mitigate NO_x emissions in aftertreatment systems [18].

Computational investigations of Cu^{II} reduction and Cu^I oxidation pathways have shed light on the mechanisms and activation barriers of processes relevant to SCR catalysis. Reduction of NH_3-solvated Cu^{II} complexes occurs via the reaction of NO and NH_3 to form H_2NNO or HONO intermediates, which further decompose to yield N_2 and H_2O products [7,11,17,19–21]. Paolucci et al. reported density functional theory (DFT) evidence that NO-assisted cleavage of an N-H bond in a bound NH_3 ligand to form an H_2NNO intermediate proceeds with similar activation energy barriers on both mononuclear $Cu^{II}(NH_3)_4$ (74 kJ mol^{-1}) and $Cu^{II}(NH_3)_3OH$ (71 kJ mol^{-1}) complexes [7,17]. The Cu^I oxidation half-cycle proceeds via reaction of two $Cu^I(NH_3)_2$ complexes with O_2 to form O_2-bridged binuclear Cu^{II} intermediates, which may require diffusion of $Cu^I(NH_3)_2$ complexes through 8-membered ring (MR) CHA

windows into adjacent CHA cages [11–14,19,22–24], as probed by Paolucci et al. using metadynamics simulations to show that $Cu^{I}(NH_3)_2$ complexes can diffuse ca. 11 Å away from an Al center into an adjacent CHA cage with a free energy barrier of ca. 55 kJ mol^{-1} [12]. DFT calculations showed that $Cu^{I}(NH_3)_2$ diffusion through an 8-MR window into an adjacent CHA cage containing a second $Cu^{I}(NH_3)_2$ complex has an activation energy barrier of 35 kJ mol^{-1}; this is followed by exothermic O_2 adsorption, suggesting that intercage Cu diffusion rather than O_2 activation limits rates of the Cu^{I} oxidation half-cycle.

The outlet exhaust gas temperature changes as a function of time during practical operation of NO_x SCR aftertreatment systems [25]. Apparent activation energies (E_{app}) describe how measured reaction rates change with temperature, and thus influence practical assessments of NO_x SCR performance often measured in the form of conversion versus temperature profiles, and E_{app} values also contain mechanistic information about the energy landscape for a catalytic cycle. This work is focused on temperature-dependent SCR reactivity in the low-temperature regime (<523 K) wherein Cu ions remain predominantly solvated by NH_3 during catalysis [7,12,26], and not in higher temperature regimes (>523 K) that lead to NH_3 de-solvation of Cu ions [7,8] and consequently higher E_{app} values (ca. 140 kJ mol^{-1} [27]) reflecting SCR reaction pathways on framework-bound Cu sites. In the low-temperature regime, E_{app} values measured on Cu-CHA zeolites at fixed gas conditions have been reported between 40–100 kJ mol^{-1} [7,11,12,16,27,28] and increase systematically with Cu ion density [11,12,16,27]. Paolucci et al. reported that E_{app} values (ca. 473 K, 0.030 kPa NO, 0.030 kPa NH_3, 10 kPa O_2, 2.5 kPa H_2O, balance N_2) increased from 47 to 74 kJ mol^{-1} as the Cu ion density in CHA (Si/Al = 15) increased from 0.03 to 0.41 Cu per 10^3 Å^3 [12]. Similarly, Gao et al. reported that E_{app} values (<473 K, 0.035 kPa NO, 0.035 kPa NH_3, 14 kPa O_2, 2.5 kPa H_2O, balance N_2) increase from ca.

40 to ca. 85 kJ mol^{-1} as the Cu ion density in CHA increased from <0.04 to 0.78 Cu per 10^3 Å^3 [11,27]. This increase in E_{app} values with Cu density appears to correspond to a transition from dual-site Cu^I oxidation to single-site Cu^{II} reduction as the dominant kinetically relevant step, as evidenced by steady-state Cu^I fractions (measured by XAS) and O_2 reaction orders that decrease with increasing Cu density at fixed reaction conditions [12]. Such data are often interpreted using mean-field kinetic treatments wherein barriers associated with each half-cycle are assumed to be independent of Cu site density, which would suggest that Cu^I oxidation has a lower E_{app} than Cu^{II} reduction [11,12,27]. In other contexts, variations (or lack thereof) in E_{app} values as a function of catalyst and SCR gas compositions have been interpreted as reflecting changes (or lack thereof) to the kinetic relevance of elementary steps such as Cu ion diffusion and O_2 activation within the Cu^I oxidation half-cycle [28]. These prevailing literature interpretations of E_{app} values implicitly assume that they solely reflect the kinetic regime under which SCR rates are measured, and are independent of active site density. However, SCR rate measurements at fixed gas conditions convolute the potentially distinct influences of kinetic regime and active site density, obscuring the underlying dependences of E_{app} values for Cu^I oxidation and Cu^{II} reduction steps on Cu ion density.

Prior work to isolate the kinetic behavior of Cu^I oxidation and Cu^{II} reduction processes on Cu-CHA materials of varying Cu ion density involved studies in which the O_2 pressure was varied widely (0–60 kPa) to alter the kinetic relevance of Cu^I oxidation and Cu^{II} reduction steps during steady-state SCR [26]. With increasing O_2 pressure, *operando* XAS showed that the most abundant reactive intermediate (MARI) transitions from NH_3-solvated Cu^I to NH_3-solvated Cu^{II} species [26,29]. Consistent with this observation, XAS measurements during NO_x SCR catalysis have shown that Cu oxidation states increase with position in the catalyst bed due to the

increasing oxidant-to-reductant ratio as a function of NO conversion [30,31], and oscillations in the oxidant-to-reductant gas ratio induce oscillations to Cu oxidation states [32]. Oda et al. monitored Cu species using *in situ* UV-visible spectroscopy in the presence of SCR gases (NO, NH_3, O_2) and observed that bands assigned to binuclear O_2-bridged Cu intermediates increased in intensity with O_2 pressure [33]. Jones et al. measured SCR rates at varying O_2 pressures and fitted them to a Langmuirian model to extract rate constants associated with Cu^I oxidation and Cu^{II} reduction [26], reporting that Cu^I oxidation rate constants (per Cu, 473 K) increase systematically with Cu density as expected from the dual-site requirement for the Cu^I oxidation step, and that Cu^{II} reduction rate constants (per Cu, 473 K) decrease with a weakly positive dependence on Cu density due to the residual influence of a changing fraction of Cu ions that are able to form binuclear intermediates. This mean-field kinetic modeling approach (i.e., rates normalized per total Cu) to analyzing Cu^I oxidation and Cu^{II} reduction rates is inherently non-rigorous in that NO_x SCR catalysis displays non-mean-field kinetic behavior resulting from the dynamic interconversion of mononuclear and binuclear NH_3-solvated Cu ions, whose mobility within zeolitic voids is restricted by electrostatic tethering to charge-balancing framework anionic centers at Al sites [12,18]. Nevertheless, as espoused by Boudart [34], such mean-field approaches to quantify catalytic turnover rates (normalized per purported active site) enable detecting deviations from the kinetic behavior expected of identical, non-interacting sites, and provide a roadmap to identify and interpret non-mean-field kinetic behavior [35].

Here, we further explore the non-mean-field nature of low-temperature NO_x SCR catalysis by measuring E_{app} values for Cu^I oxidation and Cu^{II} reduction half-cycles on Cu-CHA zeolites from steady-state SCR rate measurements across varying O_2 pressures (1–60 kPa) and temperatures (446–501 K), and determining the dependence of E_{app} values on Cu ion density.

Contrary to prevailing literature interpretations of E_{app} values estimated from SCR rate data measured at fixed gas conditions and assumed to be site-density independent, we report that E_{app} values for both Cu^{I} oxidation and Cu^{II} reduction increase with Cu ion density, and more strongly for Cu^{I} oxidation than for Cu^{II} reduction. Moreover, changes in reaction temperature are predicted to weakly influence the extent to which Cu^{I} oxidation and Cu^{II} reduction processes limit SCR rates in the low-temperature regime. Furthermore, changes to E_{app} values with active site density in a given kinetic regime are inconsistent with mean-field kinetic descriptions, implying that both Cu^{I} oxidation and Cu^{II} reduction half-cycles are sensitive to the mobility and proximity of Cu ions.

2. Methods

Details concerning CHA zeolite synthesis, Cu aqueous ion exchange, identification of the CHA topology by X-ray diffraction (XRD) (Fig. S1, SI), micropore volumes by Ar adsorption (Fig. S2, SI), elemental analysis by inductively coupled plasma optical emission spectroscopy (ICP-OES), and titration of H^{+} sites on H-form and Cu-form zeolites by NH_3-temperature programmed desorption (TPD) (Table S1, SI) are provided in the Supporting Information (Sections S.1–S.2, SI).

NO_x selective catalytic reduction (SCR) kinetic data were measured using a tubular quartz reactor system described previously [16]. Zeolite materials were sieved to obtain particle sizes between 125–250 μm in diameter. A bed height of approximately 1 cm was obtained by diluting with silica gel (Davisil, 250–500 μm in diameter). NO conversions were kept below 20% to ensure a nearly constant gas concentration across the catalyst bed, using a reactant gas composition of 0.03 kPa NO (3.5% NO/Ar, Praxair), 0.03 kPa NH_3 (3.0% NH_3/Ar, Praxair), 7

kPa CO_2 (liquid, Indiana Oxygen), 1–60 kPa O_2 (99.5%, Indiana Oxygen), 1 kPa H_2O (deionized, 18.2 MΩ cm, introduced through a 24'' Perma Pure MH Nafion™ Series Humidifier), and balance N_2 (boil-off from a liquid N_2 dewar) at ambient total pressure. The balance N_2 was composed of two independent gas streams, one which passed through the humidifier and was used as a carrier to maintain gas-phase water partial pressures at 1 kPa ("wet" N_2) and another which was used as a carrier for other gas-phase reactants ("dry" N_2). The 3.5% NO/Ar stream was pre-diluted by the "wet" N_2 carrier stream and CO_2 prior to mixing with the pure O_2 stream, to mitigate background NO_2 formation that occurs upon mixing of concentrated NO and O_2 streams. The total gas flow rate was 16.7–41.7 $cm^3\ s^{-1}$ (at ambient temperature and pressure) and the mass of CHA solids was 0.0099–0.0605 g , chosen to maintain differential NO conversion. Outlet NO, NO_2, NH_3, CO_2, and H_2O concentrations were measured every 0.95 s using on-board gas calibration and a gas-phase Fourier Transform Infrared (FTIR) spectrometer (MKS Multigas™ 2030). The rate of NO consumption was calculated according to:

$$-r_{NO} = \frac{(y_{NO,in} - y_{NO,out})}{10^6} \frac{P\dot{V}_{total}}{RT} \tag{1}$$

where y is the volume fraction of NO in ppm, $\dot{V}_{total}$ is the total volumetric flow rate, P is the ambient pressure, T is the ambient temperature, and R is the gas constant.

The rate of "standard" SCR (Eq. 2) was determined by correcting the overall rate of NO consumption measured in each experiment for contributions to NO consumption resulting from "fast" SCR (Eq. 3) reactions with NO_2, present both as an impurity in NO gas cylinders and formed via gas-phase NO oxidation reactions within the reactor unit (details reported in our previous work [26]).

$$4\,NH_3 + 4\,NO + O_2 \rightarrow 4\,N_2 + 6\,H_2O \tag{2}$$

$$4\,NH_3 + 2\,NO + 2\,NO_2 \rightarrow 4\,N_2 + 6\,H_2O \tag{3}$$

We additionally validated that NO_2 outlet concentrations measured in a blank reactor containing only SiO_2 gel change by <10% when the reactor temperature is changed from 446–501 K (at fixed gas conditions), consistent with reported E_{app} values for gas-phase NO oxidation to NO_2 that are near 0 kJ mol^{-1} [36]. Thus, we used the NO_2 concentration measured in a blank reactor at a fixed temperature of 473 K, while varying gas flow rates, O_2 pressures, and NO pressures [26], to quantitatively correct the rate of NO consumption for contributions from "fast" SCR and thus calculate the rate of "standard" SCR. The magnitude of this correction factor as a function of O_2 pressure (473 K) is shown for representative samples of lower (Cu-CHA-0.034) and higher (Cu-CHA-0.035) Cu density in Fig. S4 (SI). SCR rates are nearly independent of the reactant gas flow rate, which changes the concentration of NO_2 in the reactor formed via gas-phase NO oxidation [26], providing evidence that trace NO_2 contaminants do not significantly influence measured rate data. Additionally, calculating SCR rates without applying the correction factor for "fast" SCR does not change the trend in E_{app} values when comparing representative samples of low and high Cu density (Table S2, SI). However, we cannot rule out more complex influences of NO_2 on SCR rates, such as *in situ* generation and consumption of NO_2 at the catalyst surface, given that "fast" SCR reactions involving NO_2 as the oxidant have different active site requirements than "standard" SCR pathways involving O_2 as the oxidant [12].

Measured SCR rates were independent of space velocity and thus insensitive to external transport artifacts, as reported in our prior work [26]. Measured SCR rates were also found to be uncorrupted by intracrystallite transport artifacts according to the Weisz-Prater criterion [37], as reported in our previous work [26]. SCR rates were shown to be independent of H_2O (0.2–4 kPa) [12,38] and CO_2 (0–16 kPa) [16,38] pressures in our previous work. Apparent reaction orders in O_2 were measured by varying O_2 pressure from 1–4 kPa (a range of 2–5 kPa was used for Cu-

Cu-CHA-0.065, Cu-CHA-0.084 and Cu-CHA-0.10), 5–15 kPa and 40–60 kPa, respectively, while maintaining differential conversion and holding other gas pressures constant (0.030 kPa NO, 0.030 kPa NH_3, 1 kPa H_2O, 7 kPa CO_2 in balance N_2 at 473 K). Apparent reaction orders in NO were measured by varying NO pressure from 0.0075–0.06 kPa while maintaining differential conversion and holding other gas pressures constant (1, 10, or 60 kPa O_2; 0.030 kPa NH_3, 1 kPa H_2O, 7 kPa CO_2 in balance N_2 at 473 K). Apparent reaction orders in NH_3 were measured by varying NH_3 pressure from 0.015–0.090 kPa while maintaining differential conversion and holding other gas pressures constant (1, 10, or 60 kPa O_2; 0.030 kPa NO, 1 kPa H_2O, 7 kPa CO_2 in balance N_2 at 473 K). The logarithm of SCR reaction rates was plotted against the logarithm of reactant pressure and regressed to a linear function, whose slope was taken as the apparent reaction order. For E_{app} measurements on a given Cu-CHA sample, SCR rates at varying O_2 pressures were measured at four or five different temperatures, typically ca. 10 K apart, within the temperature range 446–501 K. SCR rates were measured at a fixed temperature while varying the O_2 pressure in a non-monotonic order, before changing to a different reaction temperature, which also varied in a non-monotonic order. The space velocity was adjusted to maintain differential conversion of NO and NH_3, with higher space velocities used at higher reaction temperatures.

E_{app} values for Cu^{I} oxidation and Cu^{II} reduction, and rate constants at a reference temperature (473 K) for Cu^{I} oxidation and Cu^{II} reduction, were computed by non-linear regression of experimental rate data to a kinetic model, as described in Section 3. Model fitting was performed in the OriginPro2020 software package by minimizing the sum of squared absolute errors between model-predicted results and experimental data. Error bars on model-fitted parameters are computed as 95% confidence intervals, equal to 1.96× the standard error.

3. Results and Discussion

3.1. E_{app} values measured at fixed gas pressures increase systematically with Cu density

To study how Cu ion density influences the kinetics of Cu^{I} oxidation and Cu^{II} reduction processes during SCR catalysis, Cu-CHA samples were prepared at fixed framework Al content (Si/Al = 15) but with varying Cu ion densities as summarized in Table 1 (additional synthesis and characterization data reported in Sections S.1 and S.2, SI). Cu-CHA samples are denoted as Cu-CHA-X, where X indicates the mean Cu volumetric density (number of Cu atoms per 10^3 Å^3). Mean Cu volumetric densities vary from 0.065–0.35 Cu atoms per 10^3 Å^3, corresponding to approximately one Cu ion per fifteen to four CHA cages (Table 1). A suite of characterization methods described in our previous work demonstrate that this set of samples contains predominantly ion-exchanged Cu, including *operando* XANES and EXAFS spectra during steady-state SCR catalysis (473 K) that are consistent with NH_3-solvated Cu^{I} and Cu^{II} ions, *ex situ* UV-visible spectra that do not show features for Cu-oxide nanoparticles, and NH_3-TPD measurements (Table S1, SI) indicating that Cu ions exchange for either one ($Cu^{II}OH$) or two (Cu^{II}) Brønsted acid sites in the zeolite framework [12,26].

Table 1. Composition data for the Cu-CHA samples studied, reproduced with permission from Ref [26].

Sample [a]	Cu/Al	Cu wt%	Cu per CHA cage	Number of cages per Cu
Cu-CHA-0.065	0.07	0.46	0.050	20.0
Cu-CHA-0.084	0.09	0.59	0.065	15.4
Cu-CHA-0.10	0.10	0.69	0.075	13.3
Cu-CHA-0.17	0.18	1.21	0.13	7.5
Cu-CHA-0.23	0.24	1.60	0.18	5.7
Cu-CHA-0.29	0.31	2.04	0.22	4.5
Cu-CHA-0.31	0.33	2.16	0.24	4.2
Cu-CHA-0.35	0.37	2.47	0.27	3.7

[a] Samples denoted Cu-CHA-X, where X = Cu volumetric density (per 10^3 Å^3).

Fig. 1 shows that E_{app} values estimated from SCR rate data measured at fixed gas conditions (10 kPa O_2) increase with Cu density, consistent with prior reports [11,12,27]. At fixed gas conditions, measured O_2 reaction orders (473 K) decrease with increasing Cu density, which reflects the decreasing kinetic relevance of dual-site Cu^I oxidation steps and the increasing kinetic relevance of single-site Cu^{II} reduction steps. E_{app} values are found to correlate with the O_2 reaction order (Fig. S5, SI); assuming a single E_{app} value for Cu^I oxidation and Cu^{II} reduction that is independent of Cu density, these data would imply a lower E_{app} value for Cu^I oxidation (37 ± 10 kJ mol^{-1}) than for Cu^{II} reduction (116 ± 12 kJ mol^{-1}) corresponding to the linear correlation in Fig. S5 (SI). Yet, the mean-field assumption that E_{app} values for Cu^I oxidation and Cu^{II} reduction are independent of Cu density may be invalid, given that rate constants for Cu^I oxidation and Cu^{II} reduction steps (per Cu, 473 K) depend on Cu ion density and thus reflect non-mean-field kinetic behavior [26]. Kinetic measurements at fixed gas conditions (Fig. 1) convolute effects due to the changing relevance of each redox half-cycle and the changing Cu ion density, motivating additional kinetic measurements to directly determine the underlying dependences of Cu^I oxidation and Cu^{II} reduction E_{app} values on Cu ion density.

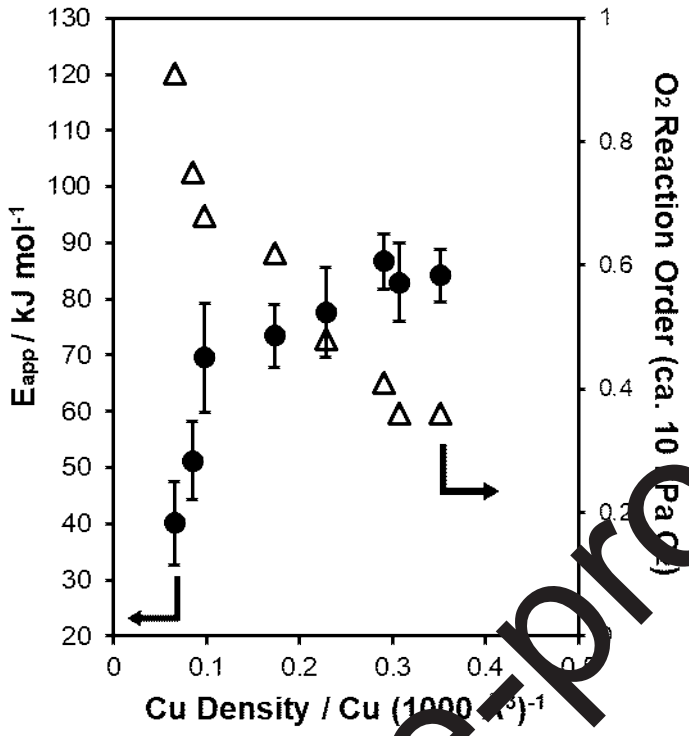

Figure 1. E_{app} values measured at fixed gas conditions (measured at four or five temperatures between 446–501 K, 10 kPa O_2, 0.030 kPa NO, 0.030 kPa NH_3, 7 kPa CO_2, 1 kPa H_2O, balance N_2) and O_2 reaction orders (473 K, ca. 10 kPa O_2) on samples of varying Cu density. Error bars on E_{app} values represent 95% confidence intervals associated with best-fit regression of the data to the Arrhenius equation.

3.2. Isolating rate constants for Cu^I oxidation and Cu^{II} reduction as a function of temperature and Cu density

To isolate the kinetic behavior of Cu^I oxidation and Cu^{II} reduction half-cycles, SCR rates were measured with widely varying O_2 pressure to change the kinetic relevance of each half-cycle. We showed previously that both the O_2 reaction order and the steady-state Cu^I fraction measured by *operando* XAS decrease with increasing O_2 pressure (Fig. S6a, SI), confirming that Cu^I oxidation becomes less kinetically relevant and Cu^{II} reduction becomes more kinetically relevant with increasing O_2 pressure [26]. SCR rates measured as a function of O_2 pressure (1–60 kPa) and at different temperatures (446–501 K) on Cu-CHA-X samples of varying Cu density in

Fig. 2. Fig. 2 shows that SCR rates display a Langmuirian dependence on O_2 pressure on Cu-CHA samples of varying Cu density and at different temperatures. SCR rates (per Cu) at a given temperature increase with Cu ion density among Cu-CHA samples, consistent with prior observations in the literature and also shown in Fig. S6b (SI) at a fixed temperature of 473 K [11,12,26,27]. At a fixed O_2 pressure within the range 1–60 kPa O_2, Cu-CHA samples of higher Cu density show a weaker dependence on O_2 pressure, as evidenced by O_2 reaction orders (473 K) that decrease with increasing Cu density (Table S3, SI) [26]. O_2 reaction orders are typically fractional and vary with Cu density, indicating that rate measurements at any fixed O_2 pressure within this range (1–60 kPa O_2) do not rigorously allow extracting kinetic information about the Cu^{I} oxidation- and Cu^{II} reduction-limited kinetic regimes. Thus, measured rate data were regressed to a Langmuirian rate expression (Eq. 4) to extract rate constants in kinetic regimes that are first-order in O_2 and thus limited by Cu^{I} oxidation (k_{first}), or zero-order in O_2 and thus limited by Cu^{II} reduction (k_{zero}) [26].

$$\frac{r_{NO}}{[Cu_{tot}]} = \frac{k_{first} k_{zero} P_{O_2}}{k_{zero} + k_{first} P_{O_2}} \tag{4}$$

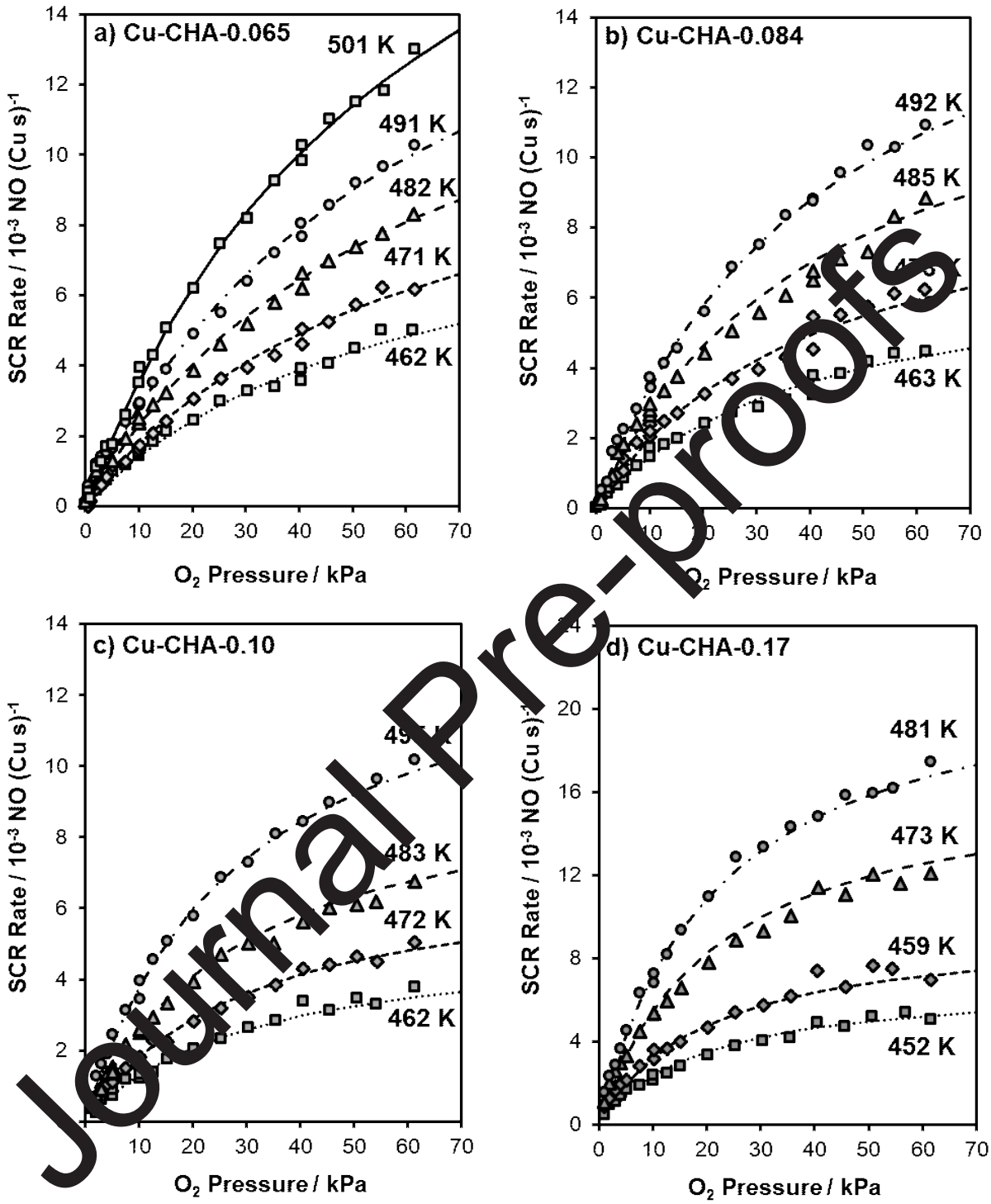

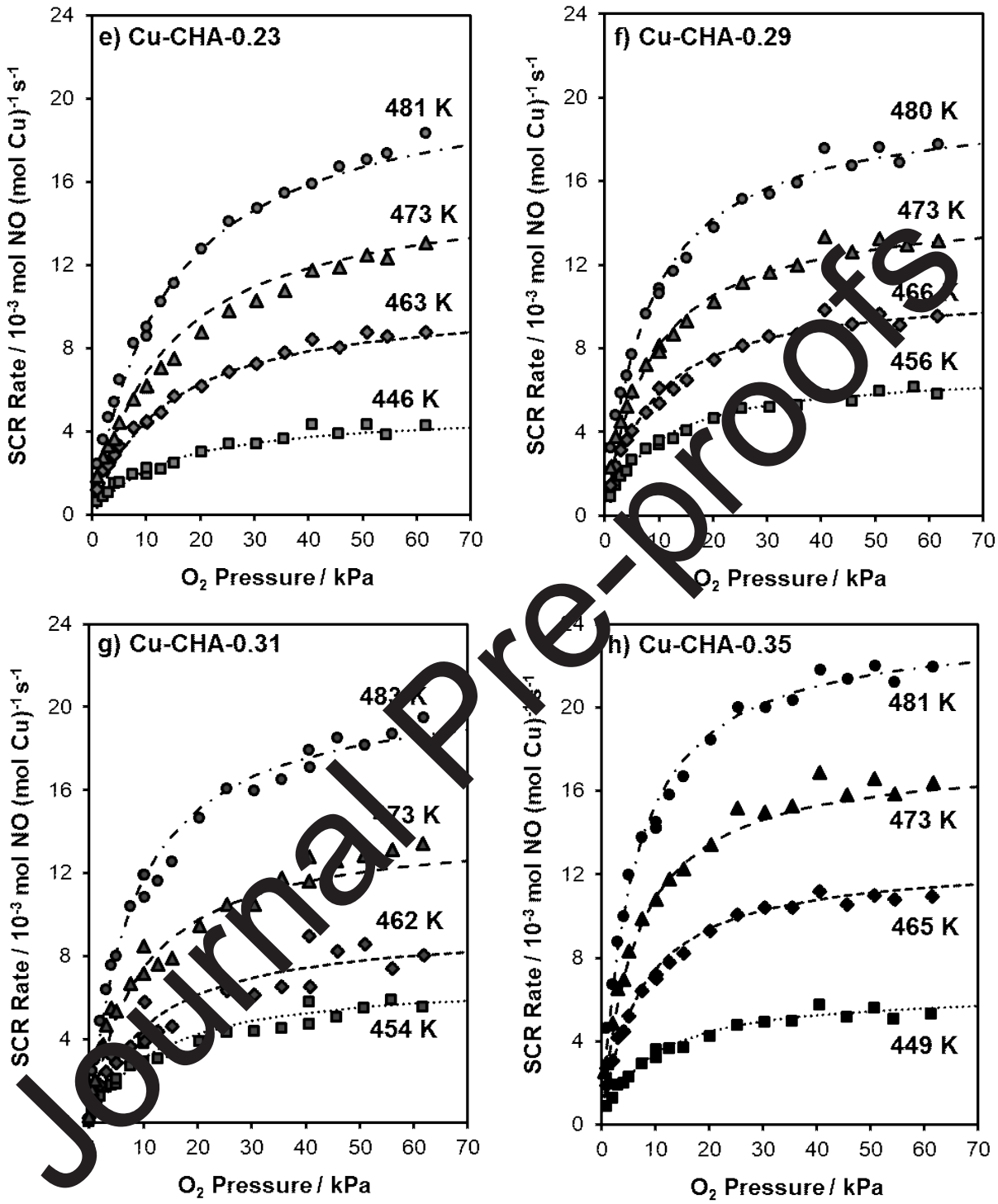

Figure 2. Steady-state SCR rates (per Cu, 473 K) as a function of O_2 pressure on Cu-CHA-X samples (panels a–h; "X" increases with light-to-dark shading) in the temperature range 446–501 K (0.030 kPa NO, 0.030 kPa NH_3, 7 kPa CO_2, 1 kPa H_2O, balance N_2. Dashed lines represent best-fit regression of rates to the temperature-dependent Langmuir model (Eqs. 4–6).

Eq. 4 alone can be used to extract k_{first} and k_{zero} values from experimental data at varying O_2 pressures at a fixed temperature. Using this approach, the O_2-pressure dependent rate data at each temperature (in Fig. 2) were used to construct Arrhenius plots that display the temperature dependences of k_{first} (Fig. 3a) and k_{zero} (Fig. 3b) values. Both k_{first} and k_{zero} values for all Cu-CHA-X samples display an Arrhenius dependence on temperature. Fig. 3a shows that k_{first} values (per Cu) at a given temperature systematically increase with Cu ion density, a consequence of the dual-site nature of Cu^{I} oxidation [26]. E_{app} values associated with k_{first} (i.e., $E_{app,first}$) increase with Cu ion density (Fig. S7a, SI), reflected in k_{first} values that increase more rapidly with temperature at higher Cu densities in Fig. 3a. Fig. 3b shows that k_{zero} values (per Cu) at a given temperature increase with weaker dependence on Cu ion density compared to k_{first} values, which is still consistent with a single-site Cu^{II} reduction process given that the fraction of Cu that can form binuclear intermediates in order to complete SCR turnovers increases with Cu density [26]. E_{app} values associated with k_{zero} (i.e., $E_{app,zero}$) are slightly lower only at the lowest Cu ion densities, then approach a nearly constant value (Fig. S7b, SI), reflected in k_{zero} values that have a nearly constant dependence on temperature at higher Cu densities in Fig. 3b.

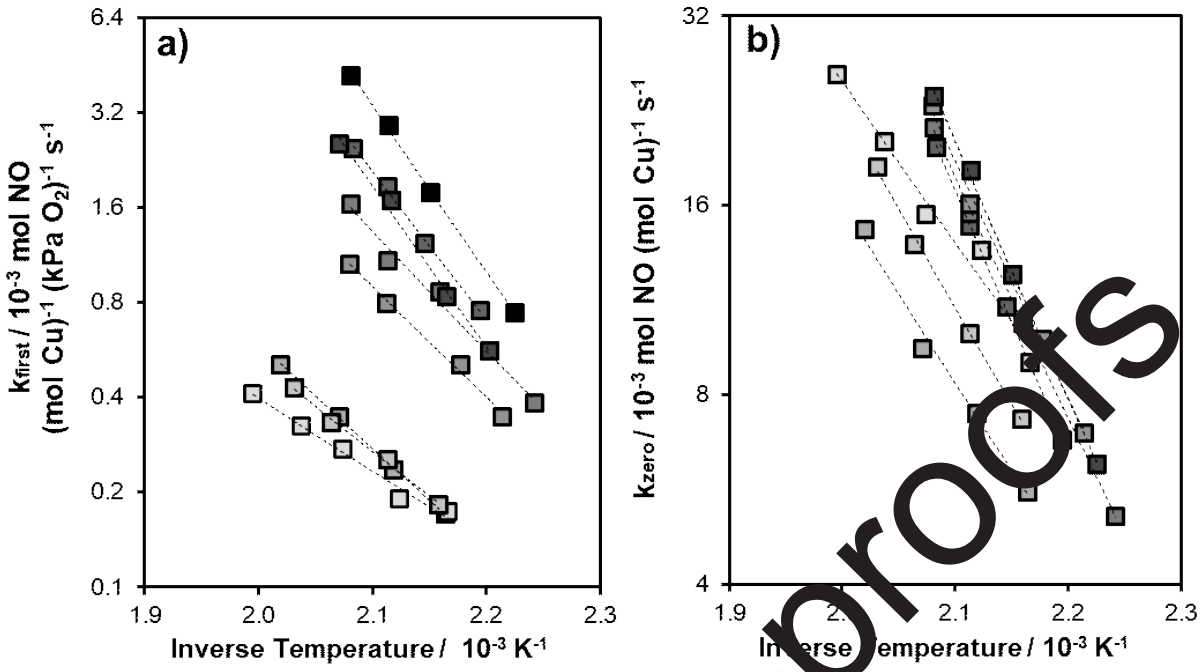

Figure 3. Dependence of a) k_{first} and b) k_{zero} values on temperature (446–501 K) on all Cu-CHA-X samples ("X" increases with light-to-dark shading) generated by fitting Eq. 4 separately to each of the O_2-pressure dependent rate data in Fig. 2. Dotted lines represent best-fit regression of rates to the Arrhenius equation (associated E_{app} values are shown in Fig. S7, SI).

The Arrhenius-dependence of k_{first} and k_{zero} values on temperature (Fig. 3) implies a single $E_{app,first}$ and a single $E_{app,zero}$ value for each Cu-CHA-X sample within the measured temperature range. Given that *operando* XAS data indicate predominantly NH_3-solvated Cu ions are present on all Cu-CHA-X samples at 473 K [12,26], these E_{app} data are consistent with active Cu ion sites that remain predominantly NH_3-solvated during SCR catalysis in the measured temperature range (446–501 K), in contrast to the NH_3 de-solvation of Cu ions observed typically at higher temperatures (>523 K) [7,8]. Significant NH_3 de-solvation would have resulted in a transition toward the higher E_{app} values characteristic of SCR reactions on zeolite-bound Cu sites (ca. 140 kJ mol^{-1}; 625–700 K [27]). Furthermore, Cu-CHA samples display NH_3 reaction orders (473 K, 15–90 Pa NH_3) that are fractional and negative (-0.4 to -0.7) at different

O_2 pressures (1, 10, or 60 kPa O_2) and Cu densities (Table S4, SI); while the mechanistic origins of NH_3 inhibition remain unclear [39–41], the lack of a systematic trend of NH_3 reaction orders (473 K) on Cu density is further evidence that Cu ion sites remain predominantly NH_3-solvated under the conditions studied.

We additionally used a temperature-dependent Langmuir model to simultaneously fit all rate data at varying O_2 pressures and temperatures on a given Cu-CHA sample (model fits shown in Fig. 2 using 473 K as the reference temperature, T_{ref}). This model includes the Langmuir functional dependence on O_2 pressure (Eq. 4) and an Arrhenius functional dependences of k_{first} and k_{zero} on temperature (Eqs. 5, 6):

$$k_{first}\,(\mathrm{T}) = k_{first,T_{ref}} \exp\left(-\frac{E_{app,first}}{R}\left(\frac{1}{T}-\frac{1}{T_{ref}}\right)\right) \tag{5}$$

$$k_{zero}\,(\mathrm{T}) = k_{zero,T_{ref}} \exp\left(-\frac{E_{app,zero}}{R}\left(\frac{1}{T}-\frac{1}{T_{ref}}\right)\right) \tag{6}$$

This model contains four fitted parameters (i.e., $k_{first,473K}$, $k_{zero,473K}$, $E_{app,first}$, $E_{app,zero}$) for each Cu-CHA sample. Values of $k_{first,473K}$ and $k_{zero,473K}$ as a function of Cu density are shown in Fig. S8 (SI), and reproduce values reported in our previous work that were determined by using the isothermal Langmuir model (Eq. 4) to fit the rate data as a function of O_2 pressure at 473 K. $E_{app,first}$ and $E_{app,zero}$ values calculated using this approach are identical, within error, to the values extracted from Fig. 3 (Fig. S7, SI) but provide a more conservative estimate of the experimental error associated with $E_{app,first}$ and $E_{app,zero}$ values.

3.3. E_{app} values for both Cu^{I} oxidation and Cu^{II} reduction depend on Cu density

As shown in Fig. 4, $E_{app,first}$ (Fig. 4a) and $E_{app,zero}$ (Fig. 4b) values extracted from the temperature-dependent Langmuir model (Eqs. 4–6) increase with Cu ion density in both Cu^{I} oxidation and Cu^{II} reduction-limited kinetic regimes, though with different functional

dependences. $E_{app,first}$ values increase monotonically with Cu density in the full range of sample compositions studied, while $E_{app,zero}$ values are invariant with Cu density except at the lowest Cu densities (0.065–0.10 Cu per 10^3 Å^3). Although these findings are consistent with E_{app} values measured at fixed gas conditions that also increase with Cu ion density (Fig. 1), Fig. 4 shows clearly that E_{app} values in limiting kinetic regimes, especially $E_{app,first}$ values, are not independent of Cu density as would be expected for mean-field kinetic behavior, an assumption implicit in prior interpretations of E_{app} data prevalent in the literature. For comparison, the experimental E_{app} data in Fig. 4 are inconsistent with a hypothetical mean-field model in which $E_{app,first}$ = 37 ± 10 kJ mol^{-1} and $E_{app,zero}$ = 116 ± 12 kJ mol^{-1}, and both parameters are independent of Cu density (shown as dotted lines in Fig. 4; extracted from Fig. S5, SI). Changes in E_{app} values with active site density in a fixed kinetic regime are inconsistent with mean-field kinetic descriptions, implying non-mean-field reactivity behavior that is sensitive to the proximity and mobility of Cu ions [35].

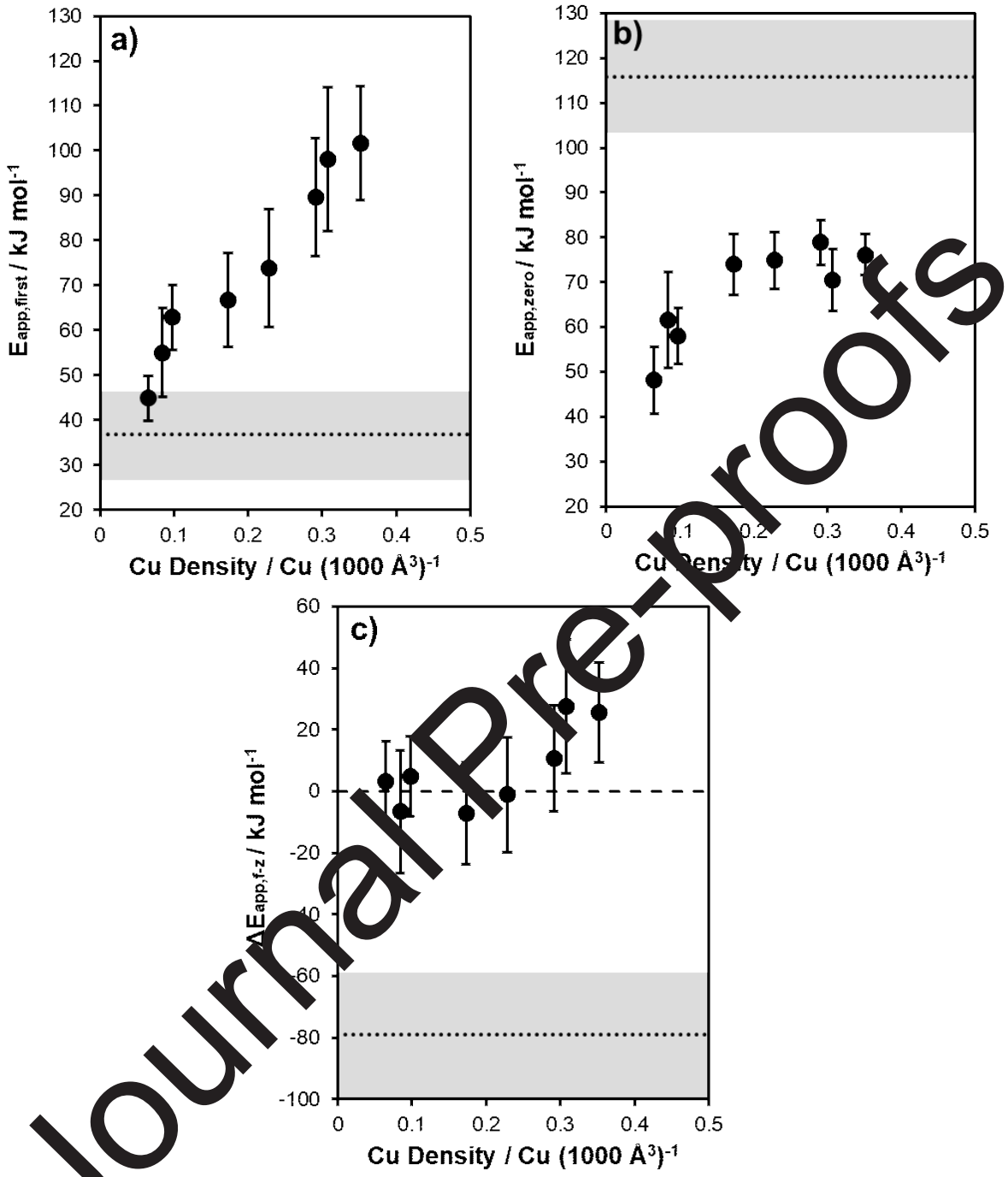

Figure 4. a) $E_{app,first}$ and b) $E_{app,zero}$ versus Cu density, computed by fitting Eqs. 4–6 to the reactivity data in Fig. 2; c) The difference $\Delta E_{app,f-z} = E_{app,first} - E_{app,zero}$ versus Cu density. Dotted lines represent a hypothetical mean-field model in which $E_{app,first} = 37 \pm 10$ kJ mol^{-1} and $E_{app,zero} = 116 \pm 12$ kJ mol^{-1} (Fig. S5, SI; 95% confidence intervals represented by gray shaded region) and are independent of Cu density. The dashed line in (c) indicates $E_{app,first} = E_{app,zero}$. Error bars represent 95% confidence intervals.

To further validate the finding that E_{app} values increase with Cu density in a fixed kinetic regime without relying on extrapolation of measured rate data to a kinetic model, E_{app} values were also estimated from rates measured directly at ca. 0.5 reaction order in O_2 (473 K) for Cu-CHA-X samples of varying Cu density (Fig. S9, SI). The O_2 pressure required to obtain an O_2 reaction order of 0.5 decreases with increasing Cu density, due to the confluence of dual-site Cu^I oxidation and single-site Cu^{II} reduction kinetics. The E_{app} values estimated using this approach also increase with Cu density, consistent with the trend in the data displayed in Fig. 4 and providing further evidence that changes to E_{app} values with Cu density at fixed gas conditions (Fig. 1) do not solely reflect a change in kinetic regime.

In the kinetic regime limited by Cu^I oxidation, $E_{app,ox}$ values increase monotonically with Cu density (Fig. 4a), suggesting that non-mean-field behavior affects Cu^I oxidation kinetics across the entire range of sample compositions studied. Steady-state XAS measurements (473 K) during SCR catalysis indicate that $Cu^I(NH_3)_2$ is the MARI in the limit of low O_2 pressure [26]. While the precise mechanistic details of the Cu^I oxidation half-cycle remain debated [12,13,22,22,23,26,29], the nearly second-order dependence of reaction rates on Cu density (Fig. S8a, SI) and first-order dependence on O_2 pressure [11,12,26,27] imply that this half-cycle involves Cu ion pairing and O_2 activation as elementary steps. DFT calculations suggest that Cu ion diffusion is kinetically relevant while O_2 activation is more facile and thus not kinetically relevant [12], analogous to proposed mechanisms for the oxidation of homogeneous Cu^I complexes via quasi-equilibrated formation of Cu-superoxide complexes followed by kinetically relevant Cu ion pairing to form O_2-bridged binuclear Cu^{II} intermediates [42,43]. *Ab initio* molecular dynamics (AIMD) simulations suggest that the free energy landscape for $Cu^I(NH_3)_2$ diffusion predominantly reflects electrostatic interactions between $Cu^I(NH_3)_2$ complexes and

framework Al anionic charges [12], such that the kinetics of Cu^{I} oxidation may be sensitive to the density and arrangement of framework Al and associated cations [18,22,28,44]. Increasing Cu ion density at fixed Al density (Si/Al = 15) systematically decreases the density of residual Brønsted acid sites, present as NH_4^+ under SCR reaction conditions [7]. The average distance between Cu ions decreases with increasing Cu density, implying a shorter diffusion distance for Cu ion pairing to occur, which should correspond to higher Cu ion pairing rates (per Cu) (Fig. S8a, 473 K). Yet, $E_{app,first}$ values increase monotonically with Cu density (Fig. 4a), suggesting an increasing enthalpic barrier for Cu ion diffusion and pairing (i.e., hindered Cu ion mobility) as NH_4^+ cations are progressively replaced by Cu cations. We note, however, that the effects of Cu and NH_4^+ densities are convoluted among Cu-CHA samples of fixed Al density, motivating future work to better understand the independent effects of Cu and Al density and arrangement on Cu ion mobility and SCR kinetics in the Cu^{I} oxidation-limited regime [18,35].

These hypotheses motivate future work to model SCR reactivity using non-mean-field kinetic treatments such as kinetic Monte Carlo (kMC) simulations that directly incorporate kinetic effects of Cu ion proximity and mobility [45,46]. We also considered the possibility that increasing Cu density decreases the kinetic relevance of Cu ion pairing steps and increases the kinetic relevance of O_2-activation steps within the Cu^{I}-oxidation half-cycle, thereby influencing $E_{app,first}$ values as a function of Cu density. However, k_{first} values (473 K) increase with Cu density throughout the range of Cu densities studied (Fig. S8a, SI) [26], implying that Cu ion pairing remains kinetically relevant throughout this composition range, given that O_2 activation kinetics should not depend on Cu density. We note that if the step forming the binuclear O_2-bridged Cu^{II} intermediate is irreversible, then the kinetics of its subsequent decomposition should not depend on O_2 pressure, and thus any influences of this reaction step on SCR kinetics would

impact k_{zero} values rather than k_{first} values. The $E_{app,first}$ values reported here are higher than those reported by Wang et al. (18 kJ mol^{-1}) in microcalorimetry measurements of the heat released as a function of time during oxidation of $Cu^{I}(NH_3)_2$ complexes in Cu-CHA (Si/Al = 14, 3.3 wt% Cu) by O_2 (0.05 kPa) in the temperature range ca. 350–473 K [47]. At this low O_2 pressure, the authors reported that only a small fraction of Cu sites oxidized in O_2 (O/Cu = 0.1, at 473 K), suggesting that the reported E_{app} value is representative of only a small fraction of the $Cu^{I}(NH_3)_2$ complexes present on the sample.

In the kinetic regime limited by Cu^{II} reduction, steady-state XAS data indicate that NH_3-solvated Cu^{II} species are the MARI (473 K), along with a fraction of unreactive $Cu^{I}(NH_3)_2$ species that cannot form binuclear O_2-bridged intermediates due to their spatial isolation from other Cu sites [12,26]. At higher Cu densities (>0.17 Cu per 10^3 Å^3), $E_{app,zero}$ values approach a fixed value of ca. 71–76 kJ mol^{-1} (Fig. 4b), similar to the DFT-calculated value for NO and NH_3-assisted single-site reduction of mononuclear NH_3-solvated Cu^{II} complexes (71–74 kJ mol^{-1}). At the lowest Cu densities (0.065–0.10 Cu per 10^3 Å^3), $E_{app,zero}$ values begin to decrease with a decrease in Cu density (Fig. 4b), suggesting that non-single-site behavior influences Cu^{II} reduction kinetics only at the lowest Cu densities. To rationalize this decrease in $E_{app,zero}$ values at the lowest Cu densities, we first consider the hypothesis that varying $E_{app,zero}$ values with Cu density reflect changes in the structure of the NH_3-solvated Cu^{II} species present during SCR catalysis. While increasing Cu density at fixed Al density (Si/Al = 15) increases the fraction of mononuclear Cu^{II} ions present as $Cu^{II}(NH_3)_3OH$ rather than $Cu^{II}(NH_3)_4$ [7] (Fig. S3, SI), reduction rate constants estimated from transient reduction of Cu^{II} species by NO and NH_3 (473 K) revealed no systematic dependence on Cu density [26], and DFT calculations suggest that $Cu^{II}(NH_3)_4$ and $Cu^{II}(NH_3)_3OH$ species have similar reduction barriers of ca. 71–74 kJ mol^{-1} [7].

Yet, the nuclearity and precise structure of NH_3-solvated Cu^{II} intermediates relevant to SCR catalysis remain unclear, and may include mononuclear Cu^{II} species and various O_2-bridged multinuclear Cu^{II} species [12,14,19–21,26]. The Cu^{II} MARI may change with Cu density among various mononuclear and binuclear structures, due to the non-mean-field nature of the (as of yet undetermined) mechanisms by which binuclear Cu^{II} complexes are reduced to mononuclear $Cu^{I}(NH_3)_2$ complexes, and such changes to the MARI structures could influence the observed trends in $E_{app,zero}$ values (Fig. 4b) if different Cu^{II} complexes have different reduction barriers. The $E_{app,zero}$ values reported in this work are higher than those reported by Gramigni et al. in transient measurements of Cu^{II} reduction of Cu-CHA (Si/Al = 12.5, 1.7 or 2.1 wt% Cu) by NO and NH_3 under H_2O co-fed conditions (25–30 kJ mol^{-1}) in the temperature range 423–493 K [20], potentially indicating a discrepancy between the reaction pathways and Cu^{II} MARI that prevail during transient reduction measurements following high temperature oxidative treatments (e.g., 723 K) [7] compared to those that prevail during steady-state catalysis. The observed trends in $E_{app,zero}$ values with Cu density (Fig. 4b) motivate future work to understand the structures of the Cu^{II} MARI under conditions of SCR catalysis as a function of Cu density, and the pathways for reduction of binuclear O-bridged NH_3-solvated Cu^{II} complexes.

Alternatively, the fraction of Cu^{I} sites that pair to form binuclear Cu^{II} intermediates under steady-state Cu reduction-limited SCR conditions could be a function of both Cu density and temperature. Given that non-pairable Cu^{I} sites are inactive spectator species during steady-state SCR catalysis [12,26], and because E_{app} values are sensitive to all temperature-dependent terms in the rate expression, changes in the fraction of pairable Cu with temperature could influence measured $E_{app,zero}$ trends (Fig. 4b). Transient measurements during O_2-assisted oxidation of $Cu^{I}(NH_3)_2$ complexes have shown that samples of lower Cu density have a lower fraction of

pairable Cu at a fixed temperature of 473 K [12,26]. This hypothesis motivates future work to quantify the fraction of pairable Cu as a function of both temperature and Cu density, and to describe the effects of Cu ion proximity and mobility using non-mean-field kinetic treatments such as kMC simulations [45,46].

Fig. 4c displays the influence of Cu ion density on the difference between $E_{app,first}$ and $E_{app,zero}$ values ($\Delta E_{app,f-z}$), which is a parameter describing the relative sensitivities of Cu^{I} oxidation and Cu^{II} reduction steps to temperature. Positive values indicate that the intrinsic rate of Cu^{I} oxidation increases more sharply with temperature than the intrinsic rate of Cu^{II} reduction, resulting in Cu^{II} reduction becoming more kinetically relevant with increasing temperature; negative values indicate the opposite trends. If the mean-field model shown in Fig. S5 (SI) that is based on E_{app} values measured at fixed gas conditions (Fig. 1) were correct, then $\Delta E_{app,f-z}$ would equal -79 ± 20 kJ mol^{-1} and be independent of Cu density (dotted line in Fig. 4c), implying that SCR rates at fixed gas pressures become progressively more limited by Cu^{I} oxidation at higher temperatures. In contrast, Fig. 4c shows that $\Delta E_{app,f-z}$ values are closer to zero than predicted by the mean-field model for any given Cu-CHA sample, such that the extent to which Cu^{I} oxidation and Cu^{II} reduction are kinetically relevant depends only weakly on temperature. At the highest Cu densities (≥ 0.11 Cu per 10^3 Å^3), $\Delta E_{app,f-z}$ values become slightly positive, because $E_{app,first}$ values continue to increase with Cu density (Fig. 4a) while $E_{app,zero}$ values do not (Fig. 4b). The weak dependence on E_{app} values on the kinetic relevance of Cu^{I} oxidation and Cu^{II} reduction steps for a given Cu-CHA sample is consistent with the findings of Ohata et al. wherein measured E_{app} values during steady-state SCR on a Cu-CHA zeolite (Si/Al = 9.5, 3.1 wt% Cu) were nearly invariant (44–49 kJ mol^{-1}) with O_2 pressure (1, 5, 15 kPa O_2) [48].

4. Conclusions

Apparent activation energies (E_{app}) measured during steady-state NO_x SCR catalysis at fixed reactant gas pressures on Cu-CHA zeolites reflect kinetic contributions from both Cu^I oxidation and Cu^{II} reduction half-cycles. The Cu^I oxidation half-cycle of low-temperature (<523 K) NO_x SCR involves the dynamic pairing of NH_3-solvated Cu^I ions to form NH_3-solvated binuclear Cu^{II} intermediates, resulting in SCR rates and E_{app} values that deviate from the mean-field behavior expected of static and non-interacting sites. Mean-field kinetic interpretations assume that E_{app} values for Cu^I oxidation and Cu^{II} reduction are independent of Cu density, implying that observed increases to E_{app} values with Cu density at fixed gas conditions solely reflect the changing kinetic relevance of these two reaction steps. In this work, steady-state SCR rate measurements across widely varying O_2 pressures (1–60 kPa) and temperatures (446–501 K) show instead that E_{app} values for Cu^I oxidation and Cu^{II} reduction processes both depend on Cu ion density. Practically, our results indicate that the extent to which Cu^I oxidation and Cu^{II} reduction steps limit SCR rates on a given Cu-CHA sample depends only weakly on temperature in the low-temperature regime characterized by NH_3-solvation of Cu sites, in contrast to prior interpretations that predict the kinetic relevance of Cu^I oxidation should increase systematically with temperature.

Mechanistically, changes in E_{app} values with active site density in a fixed kinetic regime are inconsistent with mean-field kinetic descriptions. E_{app} values for Cu^I oxidation ($E_{app,first}$) increase monotonically with Cu density, implying that non-mean-field behavior is prevalent at all Cu densities in this kinetic regime. Given that Cu ions are electrostatically tethered to anionic framework charges at Al centers, we hypothesize that this trend reflects changes to the mobility of Cu ions that interact during the Cu^I oxidation half-cycle, as charge-balancing H^+ (present as

NH_4^+ *in situ*) cations are replaced by Cu cations. This hypothesis motivates studies to unravel the separate influences of both extraframework Cu and framework Al density on Cu^I oxidation kinetics to aid in mechanistic interpretation of $E_{app,first}$ values.

E_{app} values for Cu^{II} reduction ($E_{app,zero}$) are invariant with Cu density above a threshold value (>0.17 Cu per 10^3 Å^3), consistent with mean-field kinetic behavior, but begin to deviate to lower values at the lowest Cu densities (0.065–0.10 Cu per 10^3 Å^3). Given that a variety of NH_3-solvated Cu^{II} structures may exist during SCR catalysis, changes to the structure and reduction barriers of the Cu^{II} MARI present as a function of Cu density would influence measured $E_{app,zero}$ values. Among other possibilities, the fraction of pairable Cu sites may change with both temperature and Cu density and also influence measured $E_{app,zero}$ values, motivating studies to probe the prevalence and reduction pathways of mononuclear and various binuclear Cu^{II} species during catalysis, and measure the temperature-dependence of the fraction of pairable Cu, to aid in mechanistic interpretation of $E_{app,zero}$ values.

This work reveals previously unrecognized consequences of non-mean-field kinetic behavior in NO_x SCR over Cu-zeolites, which affects not only SCR rates at fixed gas conditions and SCR rate constants for Cu^I oxidation and Cu^{II} reduction at a fixed temperature, but also the temperature dependence of such rate constants. These findings relied on identifying deviations in kinetic parameters derived from mean-field kinetic models, motivating future efforts to develop non-mean-field kinetic models to quantify how SCR reactivity depends on the mobility and proximity of electrostatically tethered Cu ions that dynamically interconvert between mononuclear and multinuclear states during steady-state catalysis. The approach used in our work follows the enduring tenets of the kinetic philosophy developed and advocated by Professor Michel Boudart to quantify and compare turnover rates, estimated from mean-field

kinetic treatments, on materials of varying active site density. Although such mean-field turnover rate values cannot rigorously describe non-mean-field kinetic behavior, this approach is advantageous in providing a systematic framework to test hypotheses about active site requirements in Cu-zeolites for NO_x SCR and other catalytic systems that display non-mean-field kinetic behavior.

Acknowledgments

We acknowledge financial support provided by the National Science Foundation DMREF program under award number 1922173-CBET. We thank Prof. William F. Schneider, Anshuman Goswami, and Yujia Wang (Notre Dame) for helpful technical discussions, and Dr. Trevor M. Lardinois for a critical review of this manuscript. We also thank Sachem, Inc. for providing the organic structure-directing agent used to synthesize SSZ-13.

Personal Acknowledgment

This manuscript is dedicated to Professor Michel Boudart, an omnipresent force who eternally inspires and guides our science.

References

[1] R. Gounder, A. Moini, Automotive NOx abatement using zeolite-based technologies, React. Chem. Eng. 4 (2019) 966–968. https://doi.org/10.1039/c9re90030f.

[2] C.K. Lambert, Perspective on SCR NOx control for diesel vehicles, React. Chem. Eng. 4 (2019) 969–974. https://doi.org/10.1039/C8RE00284C.

[3] C.H.F. Peden, Cu/Chabazite catalysts for 'Lean-Burn' vehicle emission control, J. Catal. 373 (2019) 384–389. https://doi.org/10.1016/j.jcat.2019.04.046.

[4] H. Badshah, F. Posada, R. Muncrief, Current state of NOx emissions from in-use heavy-duty diesel vehicles in the United States, International Council on Clean Transportation, 2019.

[5] T.V.W. Janssens, H. Falsig, L.F. Lundegaard, P.N.R. Vennestrøm, S.B. Rasmussen, P.G. Moses, F. Giordanino, E. Borfecchia, K.A. Lomachenko, C. Lamberti, S. Bordiga, A. Godiksen, S. Mossin, P. Beato, A Consistent Reaction Scheme for the Selective Catalytic Reduction of Nitrogen Oxides with Ammonia, ACS Catal. 5 (2015) 2832–2845. https://doi.org/10.1021/cs501673g.

[6] C. Paolucci, J.R. Di Iorio, W.F. Schneider, R. Gounder, Solvation and Mobilization of Copper Active Sites in Zeolites by Ammonia: Consequences for the Catalytic Reduction of Nitrogen Oxides, Acc. Chem. Res. 53 (2020) 1881–1892. https://doi.org/10.1021/acs.accounts.0c00328.

[7] C. Paolucci, A.A. Parekh, I. Khurana, J.R. Di Iorio, H. Li, J.D. Albarracin Caballero, A.J. Shih, T. Anggara, W.N. Delgass, J.T. Miller, F.H. Ribeiro, R. Gounder, W.F. Schneider, Catalysis in a Cage: Condition-Dependent Speciation and Dynamics of Exchanged Cu Cations in SSZ-13 Zeolites, J. Am. Chem. Soc. 138 (2016) 6028–6048. https://doi.org/10.1021/jacs.6b02651.

[8] K.A. Lomachenko, E. Borfecchia, C. Negri, G. Berlier, C. Lamberti, P. Beato, H. Falsig, S. Bordiga, The Cu-CHA deNOx Catalyst in Action: Temperature-Dependent NH3-Assisted Selective Catalytic Reduction Monitored by Operando XAS and XES, J. Am. Chem. Soc. 138 (2016) 12025–12028. https://doi.org/10.1021/jacs.6b06809.

[9] F. Giordanino, E. Borfecchia, K.A. Lomachenko, A. Lazzarini, G. Agostini, E. Gallo, A.V. Soldatov, P. Beato, S. Bordiga, C. Lamberti, Interaction of NH3 with Cu-SSZ-13 Catalyst: A Complementary FTIR, XANES, and XES Study, J. Phys. Chem. Lett. 5 (2014) 1552–1559. https://doi.org/10.1021/jz500241m.

[10] Y. Zhang, Y. Peng, K. Li, S. Liu, J. Chen, J. Li, F. Gao, C.H.F. Peden, Using Transient FTIR Spectroscopy to Probe Active Sites and Reaction Intermediates for Selective Catalytic Reduction of NOx on Cu/SSZ-13 Catalysts, ACS Catal. 9 (2019) 6137–6145. https://doi.org/10.1021/acscatal.9b00759.

[11] F. Gao, D. Mei, Y. Wang, J. Szanyi, C.H.F. Peden, Selective Catalytic Reduction over Cu/SSZ-13: Linking Homo- and Heterogeneous Catalysis, J. Am. Chem. Soc. 139 (2017) 4935–4942. https://doi.org/10.1021/jacs.7b01128.

[12] C. Paolucci, I. Khurana, A.A. Parekh, S. Li, A.J. Shih, H. Li, J.R. Di Iorio, J.D. Albarracin-Caballero, A. Yezerets, J.T. Miller, W.N. Delgass, F.H. Ribeiro, W.F. Schneider, R. Gounder, Dynamic multinuclear sites formed by mobilized copper ions in NO$_x$ selective catalytic reduction, Science. 357 (2017) 898–903. https://doi.org/10.1126/science.aan5630.

[13] L. Chen, H. Falsig, T.V.W. Janssens, H. Grönbeck, Activation of oxygen on (NH3CuNH3)+ in NH3-SCR over Cu-CHA, J. Catal. 358 (2018) 179–186. https://doi.org/10.1016/j.jcat.2017.12.009.

[14] C. Negri, T. Selleri, E. Borfecchia, A. Martini, K.A. Lomachenko, T.V.W. Janssens, M. Cutini, S. Bordiga, G. Berlier, Structure and Reactivity of Oxygen-Bridged Diamino Dicopper(II) Complexes in Cu-Ion-Exchanged Chabazite Catalyst for NH3-Mediated Selective Catalytic Reduction, J. Am. Chem. Soc. 142 (2020) 15884–15896. https://doi.org/10.1021/jacs.0c06270.

[15] V.F. Kispersky, A.J. Kropf, F.H. Ribeiro, J.T. Miller, Low absorption vitreous carbon reactors for operandoXAS: a case study on Cu/Zeolites for selective catalytic reduction of NOx by NH3, Phys. Chem. Chem. Phys. 14 (2012) 2229–2238. https://doi.org/10.1039/c1cp22992c.

[16] S.A. Bates, A.A. Verma, C. Paolucci, A.A. Parekh, T. Anggara, A. Yezerets, W.F. Schneider, J.T. Miller, W.N. Delgass, F.H. Ribeiro, Identification of the active Cu site in standard selective catalytic reduction with ammonia on Cu-SSZ-13, J. Catal. 312 (2014) 87–97.

[17] C. Paolucci, A.A. Verma, S.A. Bates, V.F. Kispersky, J.T. Miller, R. Gounder, W.N. Delgass, F.H. Ribeiro, W.F. Schneider, Isolation of the Copper Redox Steps in the Standard Selective Catalytic Reduction on Cu-SSZ-13, Angew. Chem. Int. Ed. 53 (2014) 11828–11833. https://doi.org/10.1002/anie.201407030.

[18] S.H. Krishna, C.B. Jones, J.T. Miller, F.H. Ribeiro, R. Gounder, Combining Kinetics and Operando Spectroscopy to Interrogate the Mechanism and Active Site Requirements of NOx Selective Catalytic Reduction with NH3 on Cu-Zeolites, J. Phys. Chem. Lett. 11 (2020) 5029–5036. https://doi.org/10.1021/acs.jpclett.0c00903.

[19] L. Chen, T.V.W. Janssens, P.N.R. Vennestrøm, J. Jansson, M. Skoglundh, H. Grönbeck, A Complete Multisite Reaction Mechanism for Low-Temperature NH3-SCR over Cu-CHA, ACS Catal. 10 (2020) 5646–5656. https://doi.org/10.1021/acscatal.0c00440.

[20] F. Gramigni, N.D. Nasello, N. Usberti, U. Iacobone, T. Selleri, W. Hu, S. Liu, X. Gao, I. Nova, E. Tronconi, Transient Kinetic Analysis of Low-Temperature NH3-SCR over Cu-CHA Catalysts Reveals a Quadratic Dependence of Cu Reduction Rates on CuII, ACS Catal. (2021) 4821–4831. https://doi.org/10.1021/acscatal.0c05362.

[21] W. Hu, T. Selleri, F. Gramigni, E. Fenes, K.R. Rout, S. Liu, I. Nova, D. Chen, X. Gao, E. Tronconi, On the Redox Mechanism of Low-Temperature NH3-SCR over Cu-CHA: A Combined Experimental and Theoretical Study of the Reduction Half Cycle, Angew. Chem. Int. Ed. 60 (2021) 7197. https://doi.org/10.1002/anie.202014926.

[22] L. Chen, H. Falsig, T.V.W. Janssens, J. Jansson, M. Skoglundh, H. Grönbeck, Effect of Al-distribution on oxygen activation over Cu–CHA, Catal. Sci. Technol. 8 (2018) 2131–2138. https://doi.org/10.1039/c8cy00083b.

[23] C. Liu, H. Kubota, T. Toyao, Z. Maeno, K. Shimizu, Mechanistic insights into the oxidation of copper(I) species during NH3–SCR over Cu-CHA zeolites: A DFT study, Catal. Sci. Technol. 10 (2020) 3586–3593. https://doi.org/10.1039/D0CY00379D.

[24] L. Chen, T.V.W. Janssens, H. Grönbeck, A comparative test of different density functionals for calculations of NH3-SCR over Cu-Chabazite, Phys. Chem. Chem. Phys. 21 (2019) 10923–10930. https://doi.org/10.1039/C9CP01576K.

[25] G. Cavataio, J. Girard, J.E. Patterson, C. Montreuil, Y. Cheng, C.K. Lambert, Laboratory Testing of Urea-SCR Formulations to Meet Tier 2 Bin 5 Emissions, in: SAE World Congr. Exhib., SAE International, 2007. https://doi.org/10.4271/2007-01-1575.

[26] C.B. Jones, I. Khurana, S.H. Krishna, A.J. Shih, W.N. Delgass, J.T. Miller, F.H. Ribeiro, W.F. Schneider, R. Gounder, Effects of dioxygen pressure on rates of NOx selective catalytic reduction with NH3 on Cu-CHA zeolites, J. Catal. 389 (2020) 140–149. https://doi.org/10.1016/j.jcat.2020.05.022.

[27] F. Gao, E.D. Walter, M. Kollar, Y. Wang, J. Szanyi, C.H.F. Peden, Understanding ammonia selective catalytic reduction kinetics over Cu/SSZ-13 from motion of the Cu ions, J. Catal. 319 (2014) 1–14. https://doi.org/10.1016/j.jcat.2014.08.010.

[28] H. Lee, I. Song, S.W. Jeon, D.H. Kim, Mobility of Cu Ions in Cu-SSZ-13 Determines the Reactivity of Selective Catalytic Reduction of NOx with NH3, J. Phys. Chem. Lett. (2021) 3210–3216. https://doi.org/10.1021/acs.jpclett.1c00181.

[29] C. Liu, H. Kubota, T. Amada, K. Kon, T. Toyao, Z. Maeno, K. Ueda, J. Onyama, A. Satsuma, T. Tanigawa, N. Tsunoji, T. Sano, K. Shimizu, In Situ Spectroscopic Studies on the Redox Cycle of NH3–SCR over Cu-CHA Zeolites, ChemCatChem. 12 (2020) 3050–3059. https://doi.org/10.1002/cctc.202000024.

[30] D.E. Doronkin, M. Casapu, T. Günter, O. Müller, R. Frahm, J.-D. Grunwaldt, Operando Spatially- and Time-Resolved XAS Study on Zeolite Catalysts for Selective Catalytic Reduction of NOx by NH3, J. Phys. Chem. C. 118 (2014) 10204–10212. https://doi.org/10.1021/jp5028433.

[31] Y. Murata, T. Morita, K. Wada, H. Ohno, NOx Trap Three-Way Catalyst (N-TWC) Concept: TWC with NOx Adsorption Properties at Low Temperatures for Cold-Start Emission Control, SAE Int J Fuels Lubr. 8 (2015) 454–459. https://doi.org/10.4271/2015-01-1002.

[32] A.G. Greenaway, A. Marberger, A. Thetford, I. Lezcano-González, M. Agote-Arán, M. Nachtegaal, D. Ferri, O. Kröcher, C.R.A. Catlow, A.M. Beale, Detection of key transient Cu intermediates in SSZ-13 during NH3-SCR deNOx by modulation excitation IR spectroscopy, Chem. Sci. 11 (2020) 4474–4479. https://doi.org/10.1039/c9sc04905c.

[33] A. Oda, H. Shionoya, Y. Hotta, T. Takewaki, K. Sawabe, A. Satsuma, Spectroscopic Evidence of Efficient Generation of Dicopper Intermediate in Selective Catalytic Reduction of NO over Cu-Ion-Exchanged Zeolites, ACS Catal. (2020) 12333–12339. https://doi.org/10.1021/acscatal.0c03425.

[34] M. Boudart, Turnover Rates in Heterogeneous Catalysis, Chem. Rev. 95 (1995) 661–666. https://doi.org/10.1021/cr00035a009.

[35] S.H. Krishna, C.B. Jones, R. Gounder, Dynamic Interconversion of Metal Active Site Ensembles in Zeolite Catalysis, Annu. Rev. Chem. Biomol. Eng. 12 (2021) 115–136. https://doi.org/10.1146/annurev-chembioeng-092120-010920.

[36] H. Tsukahara, T. Ishida, M. Mayumi, Gas-Phase Oxidation of Nitric Oxide: Chemical Kinetics and Rate Constant, Nitric Oxide. 3 (1999) 191–198. https://doi.org/10.1006/niox.1999.0232.

[37] P.B. Weisz, C.D. Prater, Interpretation of Measurements in Experimental Catalysis, in: W.G. Frankenburg, V.I. Komarewsky, E.K. Rideal (Eds.), Adv. Catal., Academic Press, 1954: pp. 143–196. https://doi.org/10.1016/S0360-0564(08)60390-9.

[38] A.J. Shih, I. Khurana, H. Li, J. González, A. Kumar, C. Paolucci, T.M. Lardinois, C.B. Jones, J.D. Albarracin Caballero, K. Kamasamudram, A. Yezerets, W.N. Delgass, J.T.

Miller, A.L. Villa, W.F. Schneider, R. Gounder, F.H. Ribeiro, Spectroscopic and kinetic responses of Cu-SSZ-13 to SO2 exposure and implications for NOx selective catalytic reduction, Appl. Catal. Gen. 574 (2019) 122–131. https://doi.org/10.1016/j.apcata.2019.01.024.

[39] A. Marberger, A.W. Petrov, P. Steiger, M. Elsener, O. Kröcher, M. Nachtegaal, D. Ferri, Time-resolved copper speciation during selective catalytic reduction of NO on Cu-SSZ-13, Nat. Catal. 1 (2018) 221–227. https://doi.org/10.1038/s41929-018-0032-6.

[40] A.H. Clark, R.J.G. Nuguid, P. Steiger, A. Marberger, A.W. Petrov, D. Ferri, M. Nachtegaal, O. Kröcher, Selective Catalytic Reduction of NO with NH3 on Cu−SSZ-13: Deciphering the Low and High-temperature Rate-limiting Steps by Transient XAS Experiments, ChemCatChem. 12 (2020) 1429–1435. https://doi.org/10.1002/cctc.201901916.

[41] A.R. Fahami, T. Günter, D.E. Doronkin, M. Casapu, D. Zengel, T.H. Vuong, M. Simon, F. Breher, A.V. Kucherov, A. Brückner, J.D. Grunwaldt, The dynamic nature of Cu sites in Cu-SSZ-13 and the origin of the seagull NOx conversion profile during NH3-SCR, React. Chem. Eng. 4 (2019) 1000–1018. https://doi.org/10.1039/c8re00290h.

[42] J.M. Hoover, B.L. Ryland, S.S. Stahl, Mechanism of Copper(I)/TEMPO-Catalyzed Aerobic Alcohol Oxidation, J. Am. Chem. Soc. 135 (2013) 2357–2367. https://doi.org/10.1021/ja3117203.

[43] S.D. McCann, S.S. Stahl, Copper-Catalyzed Aerobic Oxidations of Organic Molecules: Pathways for Two-Electron Oxidation with a Four-Electron Oxidant and a One-Electron Redox-Active Catalyst, Acc. Chem. Res. 48 (2015) 1756–1766. https://doi.org/10.1021/acs.accounts.5b00060.

[44] F. Gao, N.M. Washton, Y. Wang, M. Kollar, J. Szanyi, C.H.F. Peden, Effects of Si/Al ratio on Cu/SSZ-13 NH3-SCR catalyst: Implications for the active Cu species and the roles of Brønsted acidity, J. Catal. 331 (2015) 25–38. https://doi.org/10.1016/j.jcat.2015.08.004.

[45] K. Reuter, First-Principles Kinetic Monte Carlo Simulations for Heterogeneous Catalysis: Concepts, Status, and Frontiers, in: Model. Simul. Heterog. Catal. React., John Wiley & Sons, Ltd, 2011: pp. 71–111. https://doi.org/10.1002/9783527639878.ch3.

[46] M. Stamatakis, D.G. Vlachos, Unraveling the Complexity of Catalytic Reactions via Kinetic Monte Carlo Simulation: Current Status and Frontiers, ACS Catal. 2 (2012) 2648–2663. https://doi.org/10.1021/cs3005709.

[47] X. Wang, J. Chen, P.N.R. Vennestrøm, T.V.W. Janssens, J. Jansson, H. Grönbeck, M. Skoglundh, Direct measurement of enthalpy and entropy changes in NH3 promoted O2 activation over Cu-CHA at low temperature, ChemCatChem. 13 (2021) 2577. https://doi.org/10.1002/cctc.202100253.

[48] Y. Ohata, T. Ohnishi, T. Moteki, M. Ogura, High NH3-SCR reaction rate with low dependence on O2 partial pressure over Al-rich Cu–*BEA zeolite, RSC Adv. 11 (2021) 10381–10384. https://doi.org/10.1039/D1RA00943E.

Highlights

- Rates of NO_x SCR redox cycle depend on Cu ion density and kinetic regime
- Langmuirian kinetic model describes SCR rates at varying O_2 pressure and temperature

- E_{app} values for both Cu^{I} oxidation and Cu^{II} reduction depend on Cu density
- Kinetic relevance of Cu^{I} oxidation and Cu^{II} reduction depends weakly on temperature
- Changes in E_{app} with Cu ion site density reflect non-mean-field kinetic behavior

TOC Graphic

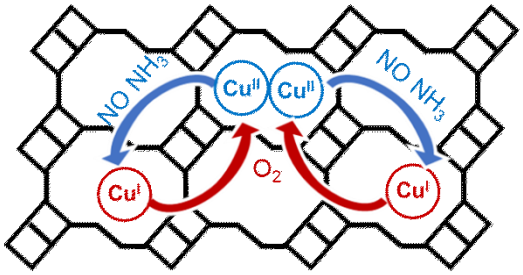

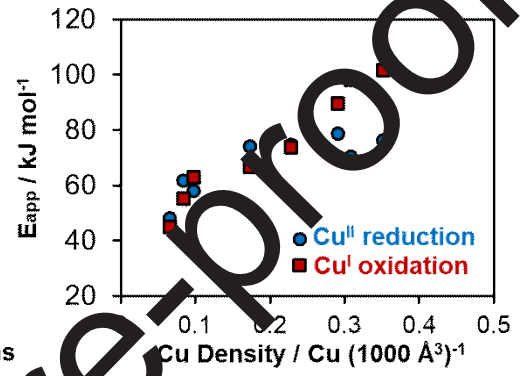

Apparent activation energies for NO_x SCR depend on Cu ion density under both Cu^{I} oxidation- and Cu^{II} reduction-limited conditions

Declaration of interests

☐ The authors declare that they have no known competing financial interests or personal relationships that could have appeared to influence the work reported in this paper.

☐The authors declare the following financial interests/personal relationships which may be considered as potential competing interests:

None.